Ultrafast population and structural dynamics of a Ni-bipyridine photoredox catalyst reveal a significant deactivation pathway

Sumana L. Raj[1,2], Felipe Curtolo[3], Kacie J. Nelson[1], David A. Cagan[4], Reagan X. Hooper[1], Daniel Bím[4], Alec H. Follmer[4], Ryan D. Ribson[4], Nathanael P. Kazmierczak[4,†], Brendon J. McNicholas[4], Natalia Powers-Riggs[1], Michael Sachs[1], Elisa Biasin[5], Dimosthenis Sokaras[6], Jinkyu Lim[2], Leland B. Gee[2], Matthieu Chollet[2], Patrick Kramer[2], Roberto Alonso Mori[2], Tim B. van Driel[2], Kelly J. Gaffney[1], Sijia S. Dong[3,7,8*], Ryan G. Hadt[4], Amy A. Cordones[1*]

[1] *Stanford PULSE Institute, SLAC National Accelerator Laboratory, Stanford University, Menlo Park, CA 94025, USA*

[2] *Linac Coherent Light Source, SLAC National Accelerator Laboratory, Menlo Park, CA, 94025, USA*

[3]*Department of Chemistry and Chemical Biology, Northeastern University, Boston, MA 02115, USA*

[4] *Division of Chemistry and Chemical Engineering, Arthur Amos Noyes Laboratory of Chemical Physics, California Institute of Technology, Pasadena, California 91125, USA*

[5]*Physical and Computational Sciences Directorate, Pacific Northwest National Laboratory, Richland, WA, USA 99354*

[6]*SSRL, SLAC National Accelerator Laboratory, Menlo Park, California 94025, USA*

[7]*Department of Physics, Northeastern University, Boston, MA 02115, USA*

[8]*Department of Chemical Engineering, Northeastern University, Boston, MA 02115, USA*

**Corresponding authors: s.dong@northeastern.edu, acordon@slac.stanford.edu*

[†]Current address: Department of Chemistry, Hope College, Holland, MI 49423, USA

Abstract

The ultrafast excited state pathways and dynamics of Ni^{II}-bipyridine complexes influence the yield of photochemical processes involved in their catalytic cross-coupling reactions. Here we present ultrafast Ni Kβ x-ray emission spectroscopy (XES) and x-ray solution scattering (XSS) of a Ni^{II}-bipyridine aryl halide complex, [Ni(*t*-^{Bu}bpy)(*o*-tol)Br], to quantify the excited state population dynamics and structural changes of the pre-catalyst. Due to the local spin-sensitivity of XES, the population dynamics of metal-to-ligand charge transfer (MLCT) and metal-centered (MC) excited states is established. A rapid ground state recovery pathway is newly identified, representing a significant deactivation pathway during photocatalysis. Furthermore, the pseudotetrahedral structure of the long-lived MC excited state is unambiguously identified and refined by XSS. The results advance our understanding of the ultrafast relaxation mechanisms that impact the photocatalytic mechanism and yield for Ni^{II}-bipyridine aryl halide cross-coupling catalysts.

TOC graphic

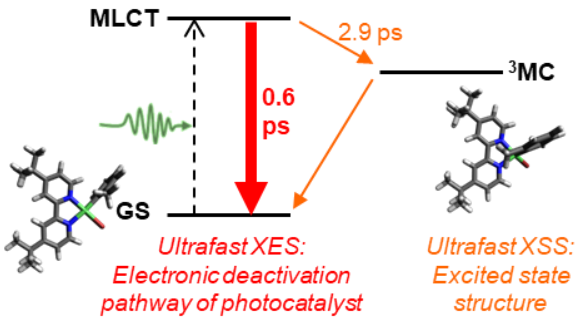

Manuscript Text

The development of first-row transition metal photocatalysts is important for achieving challenging synthetic transformations using earth abundant materials. Ni^{II}-bpy (where bpy = 2,2'-bipyridine) complexes have been widely and successfully implemented in a range of photoredox reactions driving the formation of C–C and C–heteroatom cross-coupling products.[1–5] Notably, Ni^{II}-bpy complexes can catalyze C(sp^3)–C(sp^3) cross-coupling reactions difficult to access with traditional Pd cross-coupling catalysts. When paired with a photosensitizer, the catalyst can be activated by either energy or electron transfer from the photosensitizer.[6,7] In some cases, Ni^{II}-bpy complexes can also be photoactivated through direct excitation, eliminating the necessity of a precious metal photosensitizer.[6,7] In particular, light-driven cross-coupling products have been demonstrated for Ni^{II}-bpy aryl halide [Ni(bpy)ArX] (Ar = aryl, X = halide) complexes, such as that shown in Figure 1, upon direct excitation.[8–12] The mechanism for this reaction is proposed to proceed via excited state Ni–C bond homolysis that serves as a critical entry point into a Ni^{I}/Ni^{III} catalytic cycle.[7] This has motivated several studies of the excited state dynamics of [Ni(bpy)ArX] and related complexes.[8,12–18] However, direct real-time observation of the homolysis process (and correlation with specific excited state processes leading to it) have been unachievable due to the very low quantum yield (10^{-3}-10^{-4}) for the bond breaking reaction.[14]

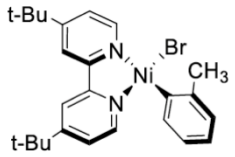

Figure 1. Molecular structure of [Ni($^{t\text{-Bu}}$bpy)(*o*-tol)Br], a representative example of [Ni(bpy)ArX] cross-coupling photocatalysts investigated here.

Optical transient absorption in the UV-Visible and IR spectral ranges have been used to assess the ultrafast excited state dynamics underpinning the photochemical reactivity of [Ni(bpy)ArX] complexes.[8,12] The prominent absorption features in the visible range correspond to Ni-to-bpy metal-to-ligand charge transfer (MLCT) excitations.[12] However, the dynamical processes following MLCT excitation have been more challenging to assign based on transient optical spectroscopies alone, as these methods are not uniquely nor directly sensitive to electronic excited state population dynamics. Transient changes in the UV-Visible spectrum suggested vibrational relaxation of the initial MLCT excited state (0.6-1.2 ps) is followed by formation (5-14 ps) of a long-lived excited state with a ~3-8 ns lifetime (range of lifetimes due to the variety of ligands and solvents measured).[12] The long-lived excited state was initially assigned as having MLCT character,[8] but was later revised to a triplet metal centered (^{3}MC) excited state (also referred to as d-d or ligand field excitations) based on additional transient IR measurements and the observed shifts in the IR signatures of CO functional groups appended to the bpy ligand.[12] A tetrahedral

structure for the ^{3}MC state was proposed based on DFT calculations. Both the ^{3}MC character and the tetrahedral structure of the long-lived species were subsequently supported by transient x-ray spectroscopy at the Ni L-edge and K-edge, respectively.[16] However, that work did not probe the early (sub-100 ps) dynamics.

The ultrafast population dynamics should play an important role in the photochemical reaction yields of [Ni(bpy)ArX] complexes. Ni-C bond homolysis was originally proposed to occur via bond weakening in the ^{3}MC excited state.[12] Subsequent multireference calculations and photochemical investigation alternatively suggested that internal conversion from the initial MLCT state to a repulsive ligand-to-metal charge transfer (LMCT) state instead drives the Ni-C bond breaking, with the low photochemical yield partially determined by the barrier between the MLCT and LMCT states.[13,14] In either mechanistic view, the lifetime and branching of the initially excited MLCT state will directly affect the photochemical activity of the catalyst. Here we directly probe the population dynamics of the MLCT and ^{3}MC excited states on the sub-20 picosecond timescale for [Ni($^{t\text{-Bu}}$bpy)(*o*-tol)Br] (Figure 1, where $^{t\text{-Bu}}$bpy = 4,4′-di-tert-butyl-2,2′-bipyridine and *o*-tol = *o*-tolyl) dissolved in tetrahydrofuran (THF). We use an excitation wavelength of 535 nm, which accesses the low-energy side of the Ni-to-bpy MLCT absorption, but does not provide sufficient photon energy to excite the proposed dissociative LMCT excited state. For the related [Ni($^{t\text{-Bu}}$bpy)(*o*-tol)Cl], this excitation wavelength did not cause measurable homolysis, but excitation on the higher energy side of the same MLCT absorption band did.[14] The population dynamics of the MLCT and ^{3}MC excited states are quantified here from Ni Kβ x-ray emission spectroscopy (XES), due to its direct sensitivity to the local Ni spin state, as described below. In parallel, the ultrafast x-ray solution scattering (XSS) is measured to track the structural changes that occur on the ^{3}MC potential energy surface and refine the tetrahedral structure of the relaxed ^{3}MC state. All measurements were conducted at the X-ray Correlation Spectroscopy (XCS) liquid jet endstation of the Linac Coherent Light Source (LCLS). Detailed experimental and computational methods are described in the Supporting Information.

Ultrafast Ni Kβ x-ray emission spectroscopy reveals excited state population dynamics

Ni Kβ x-ray emission spectroscopy (XES) probes the 3p-1s emission following ionization of a Ni 1s core electron. The Ni Kβ XES spectrum is comprised of a main Kβ$_{1,3}$ line ~8265 eV and a weaker Kβ' line ~8255 eV. The relative intensity of the Kβ' line and its energetic splitting with respect to the Kβ$_{1,3}$ line both increase with increasing 3p-3d exchange interaction.[19–22] The shape of the spectrum is therefore highly sensitive to the local spin density on the metal, which can be quantified by comparison with appropriate reference complexes. Thus, Kβ XES is widely used to determine metal spin and oxidation state changes, particularly for complexes of Fe and Mn.[23–33] In the ultrafast domain, the use of reference Kβ XES spectra to model the excited states of varied Fe spin moment has been integral for determining the mechanisms and dynamics of light induced spin crossover for numerous photoactive Fe complexes.[34–39]

Ni Kβ XES has been less widely utilized. A single comparison of Ni Kβ XES spectra for reference complexes of varied spin identified the same monotonic increase in the $K\beta_{1,3}$ line energy and Kβ' intensity that are well documented in Mn and Fe.[40] Thus, the Ni Kβ difference spectrum measured following excitation of [Ni($^{t\text{-Bu}}$bpy)(*o*-tol)Br] will reflect the changes in the local spin density on the Ni atom in the excited state and, therefore, the population dynamics of the ground state (singlet Ni^{II}), MLCT excited state (doublet Ni^{III}), and ^{3}MC excited state (triplet Ni^{II}). For this purpose, we provide additional reference complex Ni Kβ spectra, more similar to [Ni($^{t\text{-Bu}}$bpy)(*o*-tol)Br] in structure and ligation than the prior references. The reference spectra are plotted in Figure 2a-b, where [Ni($^{t\text{-Bu}}$bpy)(*o*-tol)Br] represents our singlet Ni ground state spectrum, $[Ni(cyclam)]^{3+}$ (cyclam = 1,4,8,11-tetraazacyclotetradecane) models the doublet Ni species formed in the MLCT excited state (square planar structure), and $[Ni(bis(indanyloxazoline))Br_2]$ models the triplet Ni species of the ^{3}MC excited state (tetrahedral structure). Additional reference complexes are also presented in Figure S4 to identify how variations in metal-ligand bonding impact the Ni Kβ XES spectrum.Following excitation of [Ni($^{t\text{-Bu}}$bpy)(*o*-tol)Br] in THF at 535 nm, Kβ emission spectra were measured as a function of time delay. Difference XES spectra are presented in Figure 2c-d at delays averaged over 0.2-1.2 ps delays and at 19.2 ps fixed delay. Both difference spectra show clear depletions around 8265 eV and enhanced signal around 8268 eV, consistent with increased spin density on Ni in the excited states. The 19 ps difference spectrum is best fit using the triplet Ni reference spectrum, as expected for a long-lived ^{3}MC excited state. The 0.2-1.2 ps difference spectrum is not well fit by either of the doublet or triplet Ni reference complexes alone and may represent a mixture of the two excited state populations at this delay time (Figure S3). The shape of the transient spectra below ~8262 eV is difficult to assess quantitively due to the noise level of the data. However, it is robustly observed that the absolute magnitude of the transient difference signal decreases significantly between the early and late delay times (Figure 2f). This observation is inconsistent with the increasing spin density expected for quantitative formation of ^{3}MC states from the initially populated MLCT states, which would be expected to increase the difference magnitude. Alternative photophysical pathways to explain this observation are considered below.

The time-dependence of the Kβ difference signal magnitude is shown in Figures 2e-f on two timescales. Figure 2e illustrates the prompt growth of the difference signal within the instrument response function (130±60 fs FWHM) of the experiment. Figure 2f illustrates the decay of the difference magnitude to approximately 30% of its maximum value within ~2 ps. The time-dependent signal has two possible mechanistic explanations. First, much faster formation of ^{3}MC excited states (<140 fs) than proposed by prior optical spectroscopy (5.6 ps)[12] could explain the single and prompt rise time in difference magnitude, followed by biphasic ground state recovery. This possibility is ruled out by the observation of spectral re-shaping between the 0.2-1.2 ps and 19 ps delay difference spectra, indicating that multiple excited states having distinct Ni spin moments are observed in the experiment. The remaining mechanistic explanation for the time-dependent data is illustrated in Figure 2g, where a significant ground state recovery pathway (k_2, decreasing difference magnitude) competes with formation of the ^{3}MC excited state (k_1, increasing difference magnitude). In this case, the prompt rise corresponds to excitation of the MLCT state

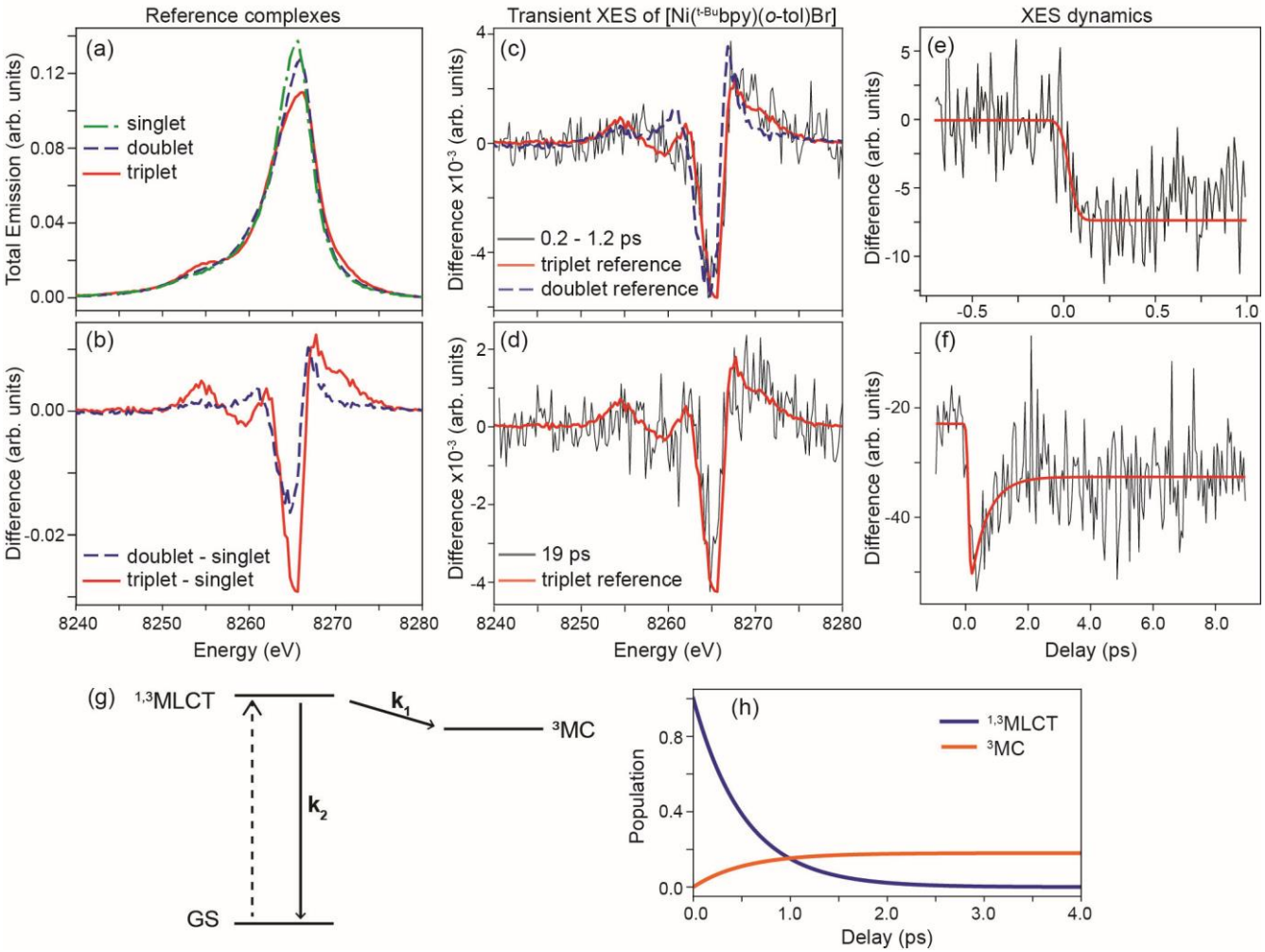

Figure 2. Ni Kβ X-ray emission spectroscopy of [Ni(*t*-^{Bu}bpy)(*o*-tol)Br] and reference complexes. (a-b) Reference complexes illustrate the expected spectra and difference spectra for singlet, doublet, and triplet Ni species. (c) Transient spectrum of [Ni(*t*-^{Bu}bpy)(*o*-tol)Br] measured over range of 0.2-1.2 ps (black) overlaid with best fit of triplet (red) and doublet (blue) reference difference spectra. (d) Transient spectrum of [Ni(*t*-^{Bu}bpy)(*o*-tol)Br] measured at 19 ps (black) overlaid with best fit of triplet (red) reference difference spectrum. (e) Early time dynamics showing the rise of x-ray emission signal integrated over range of 8263-8266 eV (black) and fit to error function (red). (f) Longer time dependence showing decay of x-ray emission signal integrated over range of 8263-8266 eV (black) and fit to kinetic model (red). (g) Kinetic model including two decay pathways for the initially excited MLCT state. (h) Population dynamics for ^{1,3}MLCT and ^{3}MC excited states extracted from the fit to the kinetic model in (g). Reported populations are relative to the initial MLCT excitation fraction.

and the longer dynamics reflect the competition between k_1 and k_2. This is the only viable explanation that allows for both the time dynamics of the difference magnitude and the time-dependent reshaping observed in the Kβ spectrum. We note, however, that we cannot exclude other short-lived intermediates in the path to ^{3}MC formation if their depletion is faster than their formation (for example, a ^{1}MC intermediate state is considered in Figure S5). Using the kinetic model of Figure 2g, the time-dependent difference magnitude can be fit to extract the excited state

population dynamics. First, time-dependent populations of the MLCT and ^{3}MC excited states are defined as follows:

$$[MLCT] = [MLCT]_0 e^{-(k_1+k_2)t} \quad 1$$

$$[MC] = [MLCT]_0 \left(\frac{k_1}{k_1+k_2}\right)\left(1 - e^{-(k_1+k_2)t}\right) \quad 2$$

The Kβ difference magnitude at a given delay can be represented by a sum of the spectral contributions of the MLCT and ^{3}MC excited states, weighted by their populations. Based on the relative magnitudes of the absolute difference signals of the doublet and triplet Ni reference complexes (Figure S2), we find that the difference magnitude of the ^{3}MC state is 1.73 times that of the MLCT state (using the same 8263-8266 eV range plotted in Figure 2e-f), such that

$$I_{XES} = S[MLCT] + 1.73S[MC] = S[MLCT]_0 \left[e^{-(k_1+k_2)t} + 1.73\left(\frac{k_1}{k_1+k_2}\right)\left(1 - e^{-(k_1+k_2)t}\right)\right] \quad 3$$

where S is a scaling factor representing the difference magnitude of the pure MLCT excited state. By fitting the time-dependent difference magnitude to Eq. 3, we find that $k_1 = 0.34 \pm 0.09$ ps^{-1} and $k_2 = 1.55 \pm 0.53$ ps^{-1} (see Table S2 for additional fit parameters). We note that the energy range used for the fit was selected to contain the maximum transient signal (and was further constrained to contain only the negative difference signal regions of the doublet and triplet reference complexes, Figure S2), but did not impact the fit results (i.e., the reported rate constants are within error of those extracted using the entire spectral range for the above analyses). We also note that the statistical uncertainty reported as error bars of the fit parameters is larger than the uncertainty introduced by the choice of specific reference complexes used in the analysis (Table S4).

The population dynamics extracted from the ultrafast Ni Kβ XES (Figure 2h) therefore identify ground state recovery as the dominant relaxation pathway (82%) following MLCT excitation of [Ni($^{t\text{-Bu}}$bpy)(*o*-tol)Br], significantly limiting formation of the ^{3}MC excited state. The timescale for formation of the ^{3}MC excited state is also mediated by the short lifetime of the MLCT state. The ^{3}MC population grows to 63% (1−1/e) of its final value within 0.55 ps, considerably faster than previously reported. Prior optical studies observed dynamics with 0.69 ps and 5.6 ps exponential time constants, which were assigned to thermalization of the MLCT excited state and ^{3}MC formation, respectively.[12] The unique sensitivity of Kβ XES to the spin moment of Ni enables the re-assignment of the faster time component to the loss of the MLCT excited state through both processes shown in Figure 2g. We speculate that the slower dynamic (observed as a blue-shift in the time-resolved IR spectroscopy of a similar complex[12]) instead probes the thermalization of the ^{3}MC state as it forms its equilibrium geometry.[41,42] The demonstration herein of very fast internal conversion to the ground state has direct implications for the yield of the Ni–C bond homolysis

reaction thought to activate the catalyst for cross-coupling reactions. As homolysis has been proposed to occur via formation of either a dissociative LMCT state or a tetrahedral ^{3}MC state following MLCT excitation,[12,13] ultrafast ground state recovery as observed here would compete with both processes. This represents a significant deactivation pathway of the excited pre-catalyst not considered previously and represents a significant limitation on the photochemical quantum yield for excited state Ni(II)–C bond homolysis.

Ultrafast X-ray Solution Scattering quantifies the tetrahedral structure of ^{3}MC excited state and its formation dynamics

Having established the excited state population dynamics of [Ni(t-^{Bu}bpy)(o-tol)Br] above, we can now utilize the x-ray solution scattering (XSS) measurements performed simultaneously to quantify the structure of the fully relaxed ^{3}MC excited state A tetrahedral structure was initially proposed based on the density functional theory (DFT) structural optimizations of the lowest energy triplet excited states of [Ni(R-bpy)(o-tol)Cl] complexes.[12] This assignment was later supported by the measurement of the transient Ni K-edge x-ray absorption spectrum at 100 ps delay time, which identified a spectral change (blueshift of the 1s-to-4p_z transition) consistent with the loss of the ground state square planar geometry in the ^{3}MC excited state.[16] However, this observation cannot definitively confirm the tetrahedral structure, as the same spectral changes have been observed both in the planar triplet excited states of Ni(II) porphyrins and phthalocyanines with expanded Ni-N bond distances, as well as upon increased coordination via axial solvent ligation.[43–48] XSS provides a more direct way to quantify the structure of the relaxed ^{3}MC state. XSS measures the elastic scattering of x-rays off all atom-pairs in the sample.[49] XSS has therefore been applied in the time domain to assess both intra-molecular structural changes of photoexcited molecules, as well as changes in their solvation structure.[49–58] Of specific interest here, the sensitivity of XSS to dihedral angle has been demonstrated previously.[53] Molecular dynamics simulations coupled with calculations of elastic x-ray scattering cross-sections have proven useful to link the XSS observables with specific structural changes,[59] and for separating different contributions to the total scattering signal from the solvent, solute, and solute-solvent components.

The isotropic difference scattering signal measured at 19 ps is shown in Figure 3a and is representative of the relaxed ^{3}MC excited state signal. The difference scattering signal is comprised of contributions from solvent-solvent, solvent-solute, and solute-solute atom pairs,[50,55] which must be deconvolved to extract the excited state structure of [Ni(t-^{Bu}bpy)(o-tol)Br]. This is accomplished here by separately considering the signals associated with THF solvent heating, taken from a reference measurement of dye in solvent in a separate experiment[60] (solvent-solvent, green trace, Figure 3a), changes in the structure of [Ni(t-^{Bu}bpy)(o-tol)Br] optimized by DFT for the lowest energy triplet excited state (solute-solute, blue trace, Figure 3a), and changes in the solvation

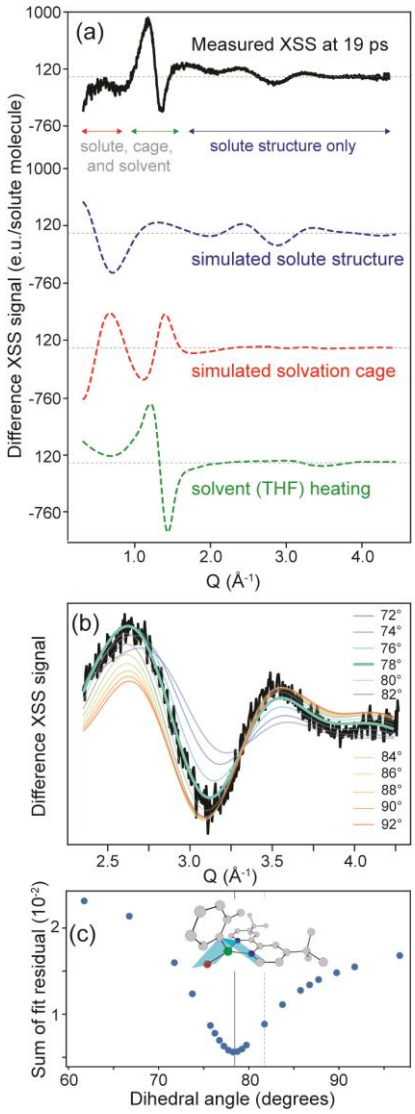

Figure 3. X-ray solution scattering (XSS) of [Ni($^{t\text{-Bu}}$bpy)(*o*-tol)Br]. (a) Experimental difference XSS measured at 19 ps delay (black, scaled to best match the simulated solute signal in the range of 2-4 Å^{-1}) and predicted difference XSS for the solute structural change (blue) and solvent cage (red) based on molecular dynamics calculations, and the solvent heating term (cyan) measured in a separate experiment and scaled to match experiment.[47] (b) The experimental XSS signal (black, 19 ps delay) in the 2-4 Å^{-1} range is compared to predicted solute structure signals as a function of dihedral angle (defined as angle between two highlighted planes, defined as 0/180° for a square planar geometry). (c) The fit residual as a function of dihedral angle suggests a structure with dihedral angle 78° (geometry index $\tau_4 = 0.80$) best describes the ^{3}MC excited state (solid line), compared to the DFT-optimized angle (dashed line).

structure surrounding [Ni($^{t\text{-Bu}}$bpy)(*o*-tol)Br] as extracted from molecular dynamics (MD) simulations (solute-solvent, red trace, Figure 3a). Additional methodological details for the calculations of the scattering signals can be found in the Supporting Information. Figure 3a shows that each difference scattering feature observed at 19 ps can be attributed to one of the three deconvolved signals. Between 1 and 1.8 Å^{-1} the difference signal is primarily attributed to heating

of the solvent and subsequent distortion of the THF solvent peak found at 1.3 $Å^{-1}$. The negative difference signal <0.5 $Å^{-1}$ suggests an increase in atomic distances that can be attributed to expansion of the solvation cage[54–56] as the [Ni(t-^{Bu}bpy)(o-tol)Br] structure changes (as supported by MD simulations of the solvation cage structure, see SI Section 5 and Figure S8). Importantly, we find that all of the difference features in the range Q >2.0 $Å^{-1}$ result from changes in the solute structure.[58]

The calculated difference scattering signal for the DFT optimized structure of the [Ni(t-^{Bu}bpy)(o-tol)Br] ^{3}MC excited state is scaled to best fit the measured 19 ps difference signal in the Q-range >2.0 $Å^{-1}$ in Figure 3b (82° simulation). From this comparison it is clear that the optimized structure provides a reasonable approximation of the excited state structure measured. The difference scattering signal is dominated by the torsional motion change in the dihedral angle from 177° (geometry index[61] τ_4=0.04) in the ground state to 82º (τ_4=0.81) in the ^{3}MC state (Figure S9), while the metal-ligand bond distances are not found to substantially impact the difference XSS signal due to their relatively small changes (Figure S7).

To specifically validate the tetrahedral structural distortion occurring for the ^{3}MC excited state, we isolate the effect of torsional motion on the scattering signal in Figure 3b by varying only the dihedral angle (defined as the angle between the N-N-C and N-C-Br planes, as shown in the Figure 3c inset). We show that as the dihedral angle approaches 90° (purple to orange in Figure 3b), all difference scattering features in this Q-range change in magnitude and shift towards lower Q values, making the difference XSS signal highly sensitive to dihedral angle. For each angle, the simulated difference XSS signal is scaled through a least-squares fit to best match the measured 19 ps difference signal and the residual is plotted in Figure 3c. The smallest residual is found for dihedral angles of 78°, providing a minor experimental refinement of the structure for the relaxed ^{3}MC excited state compared to that optimized using DFT. The structure of the ^{3}MC state best matching the XSS difference signal is reported in Table S7 and shown in Figure S9.

Taken together, the combination of Ni Kβ XES and XSS provide a complete picture for the electronic and molecular dynamics occurring in the first picoseconds following light excitation of Ni(bpy)ArX photocatalysts. We observe two dominant ultrafast relaxation pathways of the excited MLCT state. As previously reported, a ^{3}MC state is populated and its pseudotetrahedral structure was confirmed and refined here. Additionally, a dominant competing ground state recovery pathway was revealed here that was not previously reported. From the population dynamics measured herein, the lifetime of the initially populated MLCT state is considerably shorter than previously realized (~0.5 ps measured here, compared to ~5 ps concluded from prior optical work[12]). Such high energy MLCT states were predicted to initiate the photochemical Ni-C bond homolysis thought to be an important initial step in the cross-coupling reactions driven by this class of complexes.[13,14] Therefore, the ultrafast depopulation of such states measured here represents a significant deactivation pathway that limits the quantum yields of the Ni-bipyridine cross-coupling photocatalysts.

More broadly, the present results point to the direct mechanistic importance of ultrafast internal

conversion in limiting the quantum yield of light-driven bond homolysis reactions. Although quantum yield is recognized as a critical determinant of the energy costs for photoredox chemistry,[62] it is often not reported for light-driven homolysis among photocatalysts, and those that are reported vary widely from <<1% to close to 100%.[63–66] This should motivate detailed investigations of the ultrafast non-radiative internal conversion processes, such as the ground state recovery pathway identified here, that compete with the population of photochemically active (i.e., dissociative) excited states. The growing interest in these deactivating pathways is highlighted by recent work investigating the ultrafast non-radiative relaxation processes that limit the efficiency of metal-halide bond homolysis from LMCT excited states.[67] Understanding the electronic and structural properties that dictate the ultrafast branching between these active and inactive pathways will ultimately lead to the design of more efficient and cost-effective photocatalysts.

Supporting Information

Experimental methods; Ni Kβ XES supporting data and analysis; XSS supporting data and analysis; Computational methods; Calculated molecular structures; Calculation of XSS signals supporting data and analysis;

Acknowledgements

Research supported as part of BioLEC, an Energy Frontier Research Center funded by the U.S. Department of Energy (DOE), Office of Science, Basic Energy Sciences (BES), under Award # DE-SC0019370. Work by M. S. and N. P. R. was supported by the U.S. Department of Energy, Office of Basic Energy Sciences, Division of Chemical Sciences, Geosciences and Biosciences, through SLAC National Accelerator Laboratory under Contract No. DE-AC02-76SF00515. D.A.C. and N.P.K. are National Science Foundation Graduate Research Fellows (DGE-1745301). D.A.C. acknowledges support from a National Academies of Science, Engineering, and Medicine Ford Foundation Predoctoral Fellowship. N.P.K. acknowledges support from the Hertz Fellowship. This project has received funding from the European Union's Horizon 2020 research and innovation programme under the Marie Sklodowska-Curie grant agreement no. 883987 (D.B.). R.G.H. acknowledges support from the National Institutes of Health for complex synthesis and spectroscopic characterization (National Institute of General Medical Sciences, R35-GM142595). E.B. acknowledges support by the U.S. Department of Energy, Office of Science, Basic Energy Sciences, Chemical Sciences, Geosciences, and Biosciences Division, Condensed Phase and Interfacial Molecular Science program, FWP 16248. Use of the Stanford Synchrotron Radiation Lightsource, SLAC National Accelerator Laboratory, is supported by the U.S. Department of Energy, Office of Science, Office of Basic Energy Sciences under Contract No. DE-AC02-76SF00515. Use of the Linac Coherent Light Source (LCLS), SLAC National Accelerator Laboratory, is supported by the U.S. Department of Energy, Office of Science, Office of Basic

Energy Sciences under Contract No. DE-AC02-76SF00515. F.C. and S.S.D. also acknowledge Northeastern University Research Computing for providing computing resources.

References

(1) Zuo, Z.; Ahneman, D. T.; Chu, L.; Terrett, J. A.; Doyle, A. G.; MacMillan, D. W. C. Merging Photoredox with Nickel Catalysis: Coupling of α-Carboxyl Sp3-Carbons with Aryl Halides. *Science* **2014**, *345* (6195), 437–440. https://doi.org/10.1126/science.1255525.

(2) Ananikov, V. P. Nickel: The "Spirited Horse" of Transition Metal Catalysis. *ACS Catal.* **2015**, *5* (3), 1964–1971. https://doi.org/10.1021/acscatal.5b00072.

(3) Zhu, C.; Yue, H.; Chu, L.; Rueping, M. Recent Advances in Photoredox and Nickel Dual-Catalyzed Cascade Reactions: Pushing the Boundaries of Complexity. *Chem. Sci.* **2020**, *11* (16), 4051–4064. https://doi.org/10.1039/D0SC00712A.

(4) Chan, A. Y.; Perry, I. B.; Bissonnette, N. B.; Buksh, B. F.; Edwards, G. A.; Frye, L. I.; Garry, O. L.; Lavagnino, M. N.; Li, B. X.; Liang, Y.; Mao, E.; Millet, A.; Oakley, J. V.; Reed, N. L.; Sakai, H. A.; Seath, C. P.; MacMillan, D. W. C. Metallaphotoredox: The Merger of Photoredox and Transition Metal Catalysis. *Chem. Rev.* **2022**, *122* (2), 1485–1542. https://doi.org/10.1021/acs.chemrev.1c00383.

(5) Marchi, M.; Gentile, G.; Rosso, C.; Melchionna, M.; Fornasiero, P.; Filippini, G.; Prato, M. The Nickel Age in Synthetic Dual Photocatalysis: A Bright Trip Toward Materials Science. *ChemSusChem* **2022**, *15* (18), e202201094. https://doi.org/10.1002/cssc.202201094.

(6) Wenger, O. S. Photoactive Nickel Complexes in Cross-Coupling Catalysis. *Chemistry – A European Journal* **2021**, *27* (7), 2270–2278. https://doi.org/10.1002/chem.202003974.

(7) Cagan, D. A.; Bím, D.; Kazmierczak, N. P.; Hadt, R. G. Mechanisms of Photoredox Catalysis Featuring Nickel–Bipyridine Complexes. *ACS Catal.* **2024**, *14* (11), 9055–9076. https://doi.org/10.1021/acscatal.4c02036.

(8) Shields, B. J.; Kudisch, B.; Scholes, G. D.; Doyle, A. G. Long-Lived Charge-Transfer States of Nickel(II) Aryl Halide Complexes Facilitate Bimolecular Photoinduced Electron Transfer. *J. Am. Chem. Soc.* **2018**, *140* (8), 3035–3039. https://doi.org/10.1021/jacs.7b13281.

(9) Heitz, D. R.; Tellis, J. C.; Molander, G. A. Photochemical Nickel-Catalyzed C–H Arylation: Synthetic Scope and Mechanistic Investigations. *J. Am. Chem. Soc.* **2016**, *138* (39), 12715–12718. https://doi.org/10.1021/jacs.6b04789.

(10) Li, G.; Yang, L.; Liu, J.-J.; Zhang, W.; Cao, R.; Wang, C.; Zhang, Z.; Xiao, J.; Xue, D. Light-Promoted C–N Coupling of Aryl Halides with Nitroarenes. *Angewandte Chemie International Edition* **2021**, *60* (10), 5230–5234. https://doi.org/10.1002/anie.202012877.

(11) Yan, Y.; Sun, J.; Li, G.; Yang, L.; Zhang, W.; Cao, R.; Wang, C.; Xiao, J.; Xue, D. Photochemically Enabled, Ni-Catalyzed Cyanation of Aryl Halides. *Org. Lett.* **2022**, *24* (12), 2271–2275. https://doi.org/10.1021/acs.orglett.2c00203.

(12) Ting, S. I.; Garakyaraghi, S.; Taliaferro, C. M.; Shields, B. J.; Scholes, G. D.; Castellano, F. N.; Doyle, A. G. 3d-d Excited States of Ni(II) Complexes Relevant to Photoredox Catalysis: Spectroscopic Identification and Mechanistic Implications. *J. Am. Chem. Soc.* **2020**, *142* (12), 5800–5810. https://doi.org/10.1021/jacs.0c00781.

(13) Cagan, D. A.; Stroscio, G. D.; Cusumano, A. Q.; Hadt, R. G. Multireference Description of Nickel–Aryl Homolytic Bond Dissociation Processes in Photoredox Catalysis. *J. Phys. Chem. A* **2020**, *124* (48), 9915–9922. https://doi.org/10.1021/acs.jpca.0c08646.

(14) Cagan, D. A.; Bím, D.; Silva, B.; Kazmierczak, N. P.; McNicholas, B. J.; Hadt, R. G. Elucidating the Mechanism of Excited-State Bond Homolysis in Nickel–Bipyridine Photoredox Catalysts. *J. Am. Chem. Soc.* **2022**, *144* (14), 6516–6531. https://doi.org/10.1021/jacs.2c01356.
(15) Bím, D.; Luedecke, K. M.; Cagan, D. A.; Hadt, R. G. Light Activation and Photophysics of a Structurally Constrained Nickel(II)–Bipyridine Aryl Halide Complex. *Inorg. Chem.* **2024**, *63* (9), 4120–4131. https://doi.org/10.1021/acs.inorgchem.3c03822.
(16) Wallick, R. F.; Chakrabarti, S.; Burke, J. H.; Gnewkow, R.; Chae, J. B.; Rossi, T. C.; Mantouvalou, I.; Kanngießer, B.; Fondell, M.; Eckert, S.; Dykstra, C.; Smith, L. E.; Vura-Weis, J.; Mirica, L. M.; van der Veen, R. M. Excited-State Identification of a Nickel-Bipyridine Photocatalyst by Time-Resolved X-Ray Absorption Spectroscopy. *J. Phys. Chem. Lett.* **2024**, *15* (18), 4976–4982. https://doi.org/10.1021/acs.jpclett.4c00226.
(17) Cavedon, C.; Gisbertz, S.; Reischauer, S.; Vogl, S.; Sperlich, E.; Burke, J. H.; Wallick, R. F.; Schrottke, S.; Hsu, W.-H.; Anghileri, L.; Pfeifer, Y.; Richter, N.; Teutloff, C.; Müller-Werkmeister, H.; Cambié, D.; Seeberger, P. H.; Vura-Weis, J.; van der Veen, R. M.; Thomas, A.; Pieber, B. Intraligand Charge Transfer Enables Visible-Light-Mediated Nickel-Catalyzed Cross-Coupling Reactions. *Angewandte Chemie International Edition* **2022**, *61* (46), e202211433. https://doi.org/10.1002/anie.202211433.
(18) Shin, J.; Lee, J.; Suh, J.-M.; Park, K. Ligand-Field Transition-Induced C–S Bond Formation from Nickelacycles. *Chem. Sci.* **2021**, *12* (48), 15908–15915. https://doi.org/10.1039/D1SC05113J.
(19) de Groot, F. High-Resolution X-Ray Emission and X-Ray Absorption Spectroscopy. *Chem. Rev.* **2001**, *101* (6), 1779–1808. https://doi.org/10.1021/cr9900681.
(20) Glatzel, P.; Bergmann, U. High Resolution 1s Core Hole X-Ray Spectroscopy in 3d Transition Metal Complexes—Electronic and Structural Information. *Coordination Chemistry Reviews* **2005**, *249* (1), 65–95. https://doi.org/10.1016/j.ccr.2004.04.011.
(21) Bergmann, U.; Glatzel, P. X-Ray Emission Spectroscopy. *Photosynth Res* **2009**, *102* (2), 255–266. https://doi.org/10.1007/s11120-009-9483-6.
(22) DeBeer, S.; Bergmann, U. X-Ray Emission Spectroscopic Techniques in Bioinorganic Applications. In *Encyclopedia of Inorganic and Bioinorganic Chemistry*; John Wiley & Sons, Ltd, 2016; pp 1–14. https://doi.org/10.1002/9781119951438.eibc2158.
(23) Vankó, G.; Neisius, T.; Molnár, G.; Renz, F.; Kárpáti, S.; Shukla, A.; de Groot, F. M. F. Probing the 3d Spin Momentum with X-Ray Emission Spectroscopy: The Case of Molecular-Spin Transitions. *J. Phys. Chem. B* **2006**, *110* (24), 11647–11653. https://doi.org/10.1021/jp0615961.
(24) Lafuerza, S.; Carlantuono, A.; Retegan, M.; Glatzel, P. Chemical Sensitivity of Kβ and Kα X-Ray Emission from a Systematic Investigation of Iron Compounds. *Inorg. Chem.* **2020**, *59* (17), 12518–12535. https://doi.org/10.1021/acs.inorgchem.0c01620.
(25) Saveleva, V. A.; Ebner, K.; Ni, L.; Smolentsev, G.; Klose, D.; Zitolo, A.; Marelli, E.; Li, J.; Medarde, M.; Safonova, O. V.; Nachtegaal, M.; Jaouen, F.; Kramm, U. I.; Schmidt, T. J.; Herranz, J. Potential-Induced Spin Changes in Fe/N/C Electrocatalysts Assessed by In Situ X-Ray Emission Spectroscopy. *Angewandte Chemie* **2021**, *133* (21), 11813–11818. https://doi.org/10.1002/ange.202016951.
(26) Stramaglia, F.; Pugliese, G. M.; Tortora, L.; Simonelli, L.; Marini, C.; Olszewski, W.; Ishida, S.; Iyo, A.; Eisaki, H.; Mizokawa, T.; Saini, N. L. Temperature Dependence of the Local Structure and Iron Magnetic Moment in the Self-Doped CaKFe4As4 Iron-Based Superconductor. *J. Phys. Chem. C* **2021**, *125* (19), 10810–10816. https://doi.org/10.1021/acs.jpcc.1c02379.
(27) Solovyev, M.; Kucheryavy, P.; Lockard, J. V. Local Coordination and Electronic Structure Ramifications of Guest-Dependent Spin Crossover in a Metal–Organic Framework: A Combined X-Ray Absorption and Emission Spectroscopy Study. *Inorg. Chem.* **2022**, *61* (24), 9213–9223. https://doi.org/10.1021/acs.inorgchem.2c00774.

(28) Messinger, J.; Robblee, J. H.; Bergmann, U.; Fernandez, C.; Glatzel, P.; Visser, H.; Cinco, R. M.; McFarlane, K. L.; Bellacchio, E.; Pizarro, S. A.; Cramer, S. P.; Sauer, K.; Klein, M. P.; Yachandra, V. K. Absence of Mn-Centered Oxidation in the S2 → S3 Transition: Implications for the Mechanism of Photosynthetic Water Oxidation. *J. Am. Chem. Soc.* **2001**, *123* (32), 7804–7820. https://doi.org/10.1021/ja004307+.

(29) Davis, K. M.; Palenik, M. C.; Yan, L.; Smith, P. F.; Seidler, G. T.; Dismukes, G. C.; Pushkar, Y. N. X-Ray Emission Spectroscopy of Mn Coordination Complexes Toward Interpreting the Electronic Structure of the Oxygen-Evolving Complex of Photosystem II. *J. Phys. Chem. C* **2016**, *120* (6), 3326–3333. https://doi.org/10.1021/acs.jpcc.5b10610.

(30) Wang, Y.; Zhou, Z.; Wen, T.; Zhou, Y.; Li, N.; Han, F.; Xiao, Y.; Chow, P.; Sun, J.; Pravica, M.; Cornelius, A. L.; Yang, W.; Zhao, Y. Pressure-Driven Cooperative Spin-Crossover, Large-Volume Collapse, and Semiconductor-to-Metal Transition in Manganese(II) Honeycomb Lattices. *J. Am. Chem. Soc.* **2016**, *138* (48), 15751–15757. https://doi.org/10.1021/jacs.6b10225.

(31) Jensen, S. C.; Davis, K. M.; Sullivan, B.; Hartzler, D. A.; Seidler, G. T.; Casa, D. M.; Kasman, E.; Colmer, H. E.; Massie, A. A.; Jackson, T. A.; Pushkar, Y. X-Ray Emission Spectroscopy of Biomimetic Mn Coordination Complexes. *J. Phys. Chem. Lett.* **2017**, *8* (12), 2584–2589. https://doi.org/10.1021/acs.jpclett.7b01209.

(32) Wang, P.; Zhu, S.-C.; Zou, Y.; Chen, H.; Liu, Y.; Li, W.; Chen, J.; Zhu, J.; Wu, L.; Wang, S.; Yang, W.; Xiao, Y.; Chow, P.; Wang, L.; Zhao, Y. Concurrent Pressure-Induced Spin-State Transitions and Jahn–Teller Distortions in MnTe. *Chem. Mater.* **2022**, *34* (9), 3931–3940. https://doi.org/10.1021/acs.chemmater.1c04199.

(33) Wang, Y.; Bai, L.; Wen, T.; Yang, L.; Gou, H.; Xiao, Y.; Chow, P.; Pravica, M.; Yang, W.; Zhao, Y. Giant Pressure-Driven Lattice Collapse Coupled with Intermetallic Bonding and Spin-State Transition in Manganese Chalcogenides. *Angewandte Chemie International Edition* **2016**, *55* (35), 10350–10353. https://doi.org/10.1002/anie.201605410.

(34) Zhang, W.; Alonso-Mori, R.; Bergmann, U.; Bressler, C.; Chollet, M.; Galler, A.; Gawelda, W.; Hadt, R. G.; Hartsock, R. W.; Kroll, T.; Kjær, K. S.; Kubiček, K.; Lemke, H. T.; Liang, H. W.; Meyer, D. A.; Nielsen, M. M.; Purser, C.; Robinson, J. S.; Solomon, E. I.; Sun, Z.; Sokaras, D.; van Driel, T. B.; Vankó, G.; Weng, T.-C.; Zhu, D.; Gaffney, K. J. Tracking Excited-State Charge and Spin Dynamics in Iron Coordination Complexes. *Nature* **2014**, *509* (7500), 345–348. https://doi.org/10.1038/nature13252.

(35) Kinschel, D.; Bacellar, C.; Cannelli, O.; Sorokin, B.; Katayama, T.; Mancini, G. F.; Rouxel, J. R.; Obara, Y.; Nishitani, J.; Ito, H.; Ito, T.; Kurahashi, N.; Higashimura, C.; Kudo, S.; Keane, T.; Lima, F. A.; Gawelda, W.; Zalden, P.; Schulz, S.; Budarz, J. M.; Khakhulin, D.; Galler, A.; Bressler, C.; Milne, C. J.; Penfold, T.; Yabashi, M.; Suzuki, T.; Misawa, K.; Chergui, M. Femtosecond X-Ray Emission Study of the Spin Cross-over Dynamics in Haem Proteins. *Nat Commun* **2020**, *11* (1), 4145. https://doi.org/10.1038/s41467-020-17923-w.

(36) Tatsuno, H.; Kjær, K. S.; Kunnus, K.; Harlang, T. C. B.; Timm, C.; Guo, M.; Chàbera, P.; Fredin, L. A.; Hartsock, R. W.; Reinhard, M. E.; Koroidov, S.; Li, L.; Cordones, A. A.; Gordivska, O.; Prakash, O.; Liu, Y.; Laursen, M. G.; Biasin, E.; Hansen, F. B.; Vester, P.; Christensen, M.; Haldrup, K.; Németh, Z.; Sárosiné Szemes, D.; Bajnóczi, É.; Vankó, G.; Van Driel, T. B.; Alonso-Mori, R.; Glownia, J. M.; Nelson, S.; Sikorski, M.; Lemke, H. T.; Sokaras, D.; Canton, S. E.; Dohn, A. O.; Møller, K. B.; Nielsen, M. M.; Gaffney, K. J.; Wärnmark, K.; Sundström, V.; Persson, P.; Uhlig, J. Hot Branching Dynamics in a Light-Harvesting Iron Carbene Complex Revealed by Ultrafast X-Ray Emission Spectroscopy. *Angewandte Chemie* **2020**, *132* (1), 372–380. https://doi.org/10.1002/ange.201908065.

(37) Reinhard, M. E.; Mara, M. W.; Kroll, T.; Lim, H.; Hadt, R. G.; Alonso-Mori, R.; Chollet, M.; Glownia, J. M.; Nelson, S.; Sokaras, D.; Kunnus, K.; Driel, T. B. van; Hartsock, R. W.; Kjaer, K. S.;

Weninger, C.; Biasin, E.; Gee, L. B.; Hodgson, K. O.; Hedman, B.; Bergmann, U.; Solomon, E. I.; Gaffney, K. J. Short-Lived Metal-Centered Excited State Initiates Iron-Methionine Photodissociation in Ferrous Cytochrome c. *Nat Commun* **2021**, *12* (1), 1086. https://doi.org/10.1038/s41467-021-21423-w.

(38) S. Kjær, K.; Kunnus, K.; B. Harlang, T. C.; Driel, T. B. V.; Ledbetter, K.; W. Hartsock, R.; E. Reinhard, M.; Koroidov, S.; Li, L.; G. Laursen, M.; Biasin, E.; B. Hansen, F.; Vester, P.; Christensen, M.; Haldrup, K.; M. Nielsen, M.; Chabera, P.; Liu, Y.; Tatsuno, H.; Timm, C.; Uhlig, J.; Sundstöm, V.; Németh, Z.; Sárosiné Szemes, D.; Bajnóczi, É.; Vankó, G.; Alonso-Mori, R.; M. Glownia, J.; Nelson, S.; Sikorski, M.; Sokaras, D.; T. Lemke, H.; E. Canton, S.; Wärnmark, K.; Persson, P.; A. Cordones, A.; J. Gaffney, K. Solvent Control of Charge Transfer Excited State Relaxation Pathways in [Fe(2,2'-Bipyridine)(CN) 4] 2−. *Physical Chemistry Chemical Physics* **2018**, *20* (6), 4238–4249. https://doi.org/10.1039/C7CP07838B.

(39) Reinhard, M. E.; Sidhu, B. K.; Lozada, I. B.; Powers-Riggs, N.; Ortiz, R. J.; Lim, H.; Nickel, R.; Lierop, J. van; Alonso-Mori, R.; Chollet, M.; Gee, L. B.; Kramer, P. L.; Kroll, T.; Raj, S. L.; van Driel, T. B.; Cordones, A. A.; Sokaras, D.; Herbert, D. E.; Gaffney, K. J. Time-Resolved X-Ray Emission Spectroscopy and Synthetic High-Spin Model Complexes Resolve Ambiguities in Excited-State Assignments of Transition-Metal Chromophores: A Case Study of Fe-Amido Complexes. *J. Am. Chem. Soc.* **2024**, *146* (26), 17908–17916. https://doi.org/10.1021/jacs.4c02748.

(40) Glatzel, P. X-Ray Fluorescence Emission Following K Capture and 1s Photoionization of Mn and Fe in Various Chemical Environments, Hamburg University, 2001. https://www-library.desy.de/preparch/desy/thesis/desy-thesis-01-062.pdf (accessed 2024-10-24).

(41) Hamm, P.; Ohline, S. M.; Zinth, W. Vibrational Cooling after Ultrafast Photoisomerization of Azobenzene Measured by Femtosecond Infrared Spectroscopy. *J. Chem. Phys.* **1997**, *106* (2), 519–529. https://doi.org/10.1063/1.473392.

(42) Zahn, C.; Pastore, M.; Lustres, J. L. P.; Gros, P. C.; Haacke, S.; Heyne, K. Femtosecond Infrared Spectroscopy Resolving the Multiplicity of High-Spin Crossover States in Transition Metal Iron Complexes. *J. Am. Chem. Soc.* **2024**, *146* (13), 9347–9355. https://doi.org/10.1021/jacs.4c01637.

(43) Phelan, B. T.; Mara, M. W.; Chen, L. X. Excited-State Structural Dynamics of Nickel Complexes Probed by Optical and X-Ray Transient Absorption Spectroscopies: Insights and Implications. *Chem. Commun.* **2021**, *57* (90), 11904–11921. https://doi.org/10.1039/D1CC03875C.

(44) Chen, L. X.; Zhang, X.; Wasinger, E. C.; Attenkofer, K.; Jennings, G.; Muresan, A. Z.; Lindsey, J. S. Tracking Electrons and Atoms in a Photoexcited Metalloporphyrin by X-Ray Transient Absorption Spectroscopy. *J. Am. Chem. Soc.* **2007**, *129* (31), 9616–9618. https://doi.org/10.1021/ja072979v.

(45) Hong, J.; Kelley, M. S.; Shelby, M. L.; Hayes, D. K.; Hadt, R. G.; Rimmerman, D.; Zhang, X.; Chen, L. X. The Nature of the Long-Lived Excited State in a NiII Phthalocyanine Complex Investigated by X-Ray Transient Absorption Spectroscopy. *ChemSusChem* **2018**, *11* (14), 2421–2428. https://doi.org/10.1002/cssc.201800777.

(46) Chen, L. X.; Zhang, X.; Wasinger, E. C.; Lockard, J. V.; Stickrath, A. B.; Mara, M. W.; Attenkofer, K.; Jennings, G.; Smolentsev, G.; Soldatov, A. X-Ray Snapshots for Metalloporphyrin Axial Ligation. *Chem. Sci.* **2010**, *1* (5), 642–650. https://doi.org/10.1039/C0SC00323A.

(47) Hong, J.; Fauvell, T. J.; Helweh, W.; Zhang, X.; Chen, L. X. Investigation of the Photoinduced Axial Ligation Process in the Excited State of Nickel(II) Phthalocyanine. *Journal of Photochemistry and Photobiology A: Chemistry* **2019**, *372*, 270–278. https://doi.org/10.1016/j.jphotochem.2018.12.026.

(48) Colpas, G. J.; Maroney, M. J.; Bagyinka, Csaba.; Kumar, Manoj.; Willis, W. S.; Suib, S. L.; Mascharak, P. K.; Baidya, Narayan. X-Ray Spectroscopic Studies of Nickel Complexes, with

Application to the Structure of Nickel Sites in Hydrogenases. *Inorg. Chem.* **1991**, *30* (5), 920–928. https://doi.org/10.1021/ic00005a010.
(49) Ihee, H. Visualizing Solution-Phase Reaction Dynamics with Time-Resolved X-Ray Liquidography. *Acc. Chem. Res.* **2009**, *42* (2), 356–366. https://doi.org/10.1021/ar800168v.
(50) Ihee, H.; Lorenc, M.; Kim, T. K.; Kong, Q. Y.; Cammarata, M.; Lee, J. H.; Bratos, S.; Wulff, M. Ultrafast X-Ray Diffraction of Transient Molecular Structures in Solution. *Science* **2005**, *309* (5738), 1223–1227. https://doi.org/10.1126/science.1114782.
(51) Haldrup, K.; Levi, G.; Biasin, E.; Vester, P.; Laursen, M. G.; Beyer, F.; Kjær, K. S.; Brandt van Driel, T.; Harlang, T.; Dohn, A. O.; Hartsock, R. J.; Nelson, S.; Glownia, J. M.; Lemke, H. T.; Christensen, M.; Gaffney, K. J.; Henriksen, N. E.; Møller, K. B.; Nielsen, M. M. Ultrafast X-Ray Scattering Measurements of Coherent Structural Dynamics on the Ground-State Potential Energy Surface of a Diplatinum Molecule. *Phys. Rev. Lett.* **2019**, *122* (6), 063001. https://doi.org/10.1103/PhysRevLett.122.063001.
(52) van Driel, T. B.; Kjær, K. S.; Hartsock, R. W.; Dohn, A. O.; Harlang, T.; Chollet, M.; Christensen, M.; Gawelda, W.; Henriksen, N. E.; Kim, J. G.; Haldrup, K.; Kim, K. H.; Ihee, H.; Kim, J.; Lemke, H.; Sun, Z.; Sundström, V.; Zhang, W.; Zhu, D.; Møller, K. B.; Nielsen, M. M.; Gaffney, K. J. Atomistic Characterization of the Active-Site Solvation Dynamics of a Model Photocatalyst. *Nat Commun* **2016**, *7* (1), 13678. https://doi.org/10.1038/ncomms13678.
(53) Katayama, T.; Choi, T.-K.; Khakhulin, D.; O. Dohn, A.; J. Milne, C.; Vankó, G.; Németh, Z.; A. Lima, F.; Szlachetko, J.; Sato, T.; Nozawa, S.; Adachi, S.; Yabashi, M.; J. Penfold, T.; Gawelda, W.; Levi, G. Atomic-Scale Observation of Solvent Reorganization Influencing Photoinduced Structural Dynamics in a Copper Complex Photosensitizer. **2023**. https://doi.org/10.1039/D2SC06600A.
(54) Kunnus, K.; Vacher, M.; Harlang, T. C. B.; Kjær, K. S.; Haldrup, K.; Biasin, E.; van Driel, T. B.; Pápai, M.; Chabera, P.; Liu, Y.; Tatsuno, H.; Timm, C.; Källman, E.; Delcey, M.; Hartsock, R. W.; Reinhard, M. E.; Koroidov, S.; Laursen, M. G.; Hansen, F. B.; Vester, P.; Christensen, M.; Sandberg, L.; Németh, Z.; Szemes, D. S.; Bajnóczi, É.; Alonso-Mori, R.; Glownia, J. M.; Nelson, S.; Sikorski, M.; Sokaras, D.; Lemke, H. T.; Canton, S. E.; Møller, K. B.; Nielsen, M. M.; Vankó, G.; Wärnmark, K.; Sundström, V.; Persson, P.; Lundberg, M.; Uhlig, J.; Gaffney, K. J. Vibrational Wavepacket Dynamics in Fe Carbene Photosensitizer Determined with Femtosecond X-Ray Emission and Scattering. *Nat Commun* **2020**, *11* (1), 634. https://doi.org/10.1038/s41467-020-14468-w.
(55) Biasin, E.; van Driel, T. B.; Kjær, K. S.; Dohn, A. O.; Christensen, M.; Harlang, T.; Vester, P.; Chabera, P.; Liu, Y.; Uhlig, J.; Pápai, M.; Németh, Z.; Hartsock, R.; Liang, W.; Zhang, J.; Alonso-Mori, R.; Chollet, M.; Glownia, J. M.; Nelson, S.; Sokaras, D.; Assefa, T. A.; Britz, A.; Galler, A.; Gawelda, W.; Bressler, C.; Gaffney, K. J.; Lemke, H. T.; Møller, K. B.; Nielsen, M. M.; Sundström, V.; Vankó, G.; Wärnmark, K.; Canton, S. E.; Haldrup, K. Femtosecond X-Ray Scattering Study of Ultrafast Photoinduced Structural Dynamics in Solvated $[\mathrm{Co}(\mathbf{\text{terpy}}}{)}_{2}{]}^{2+}$. *Phys. Rev. Lett.* **2016**, *117* (1), 013002. https://doi.org/10.1103/PhysRevLett.117.013002.
(56) Biasin, E.; Fox, Z. W.; Andersen, A.; Ledbetter, K.; Kjær, K. S.; Alonso-Mori, R.; Carlstad, J. M.; Chollet, M.; Gaynor, J. D.; Glownia, J. M.; Hong, K.; Kroll, T.; Lee, J. H.; Liekhus-Schmaltz, C.; Reinhard, M.; Sokaras, D.; Zhang, Y.; Doumy, G.; March, A. M.; Southworth, S. H.; Mukamel, S.; Gaffney, K. J.; Schoenlein, R. W.; Govind, N.; Cordones, A. A.; Khalil, M. Direct Observation of Coherent Femtosecond Solvent Reorganization Coupled to Intramolecular Electron Transfer. *Nat. Chem.* **2021**, *13* (4), 343–349. https://doi.org/10.1038/s41557-020-00629-3.
(57) Leshchev, D.; J. S. Valentine, A.; Kim, P.; Mills, A. W.; Roy, S.; Chakraborty, A.; Biasin, E.; Haldrup, K.; Hsu, D. J.; Kirschner, M. S.; Rimmerman, D.; Chollet, M.; Glownia, J. M.; van Driel, T.

B.; Castellano, F. N.; Li, X.; Chen, L. X. Revealing Excited-State Trajectories on Potential Energy Surfaces with Atomic Resolution in Real Time. *Angewandte Chemie International Edition* **2023**, *62* (28), e202304615. https://doi.org/10.1002/anie.202304615.

(58) Leshchev, D.; B. Harlang, T. C.; A. Fredin, L.; Khakhulin, D.; Liu, Y.; Biasin, E.; G. Laursen, M.; E. Newby, G.; Haldrup, K.; M. Nielsen, M.; Wärnmark, K.; Sundström, V.; Persson, P.; S. Kjær, K.; Wulff, M. Tracking the Picosecond Deactivation Dynamics of a Photoexcited Iron Carbene Complex by Time-Resolved X-Ray Scattering. *Chemical Science* **2018**, *9* (2), 405–414. https://doi.org/10.1039/C7SC02815F.

(59) Dohn, A. O.; Biasin, E.; Haldrup, K.; Nielsen, M. M.; Henriksen, N. E.; Møller, K. B. On the Calculation of X-Ray Scattering Signals from Pairwise Radial Distribution Functions. *J. Phys. B: At. Mol. Opt. Phys.* **2015**, *48* (24), 244010. https://doi.org/10.1088/0953-4075/48/24/244010.

(60) Leshchev, D.; J. S. Valentine, A.; Kim, P.; Mills, A. W.; Roy, S.; Chakraborty, A.; Biasin, E.; Haldrup, K.; Hsu, D. J.; Kirschner, M. S.; Rimmerman, D.; Chollet, M.; Glownia, J. M.; van Driel, T. B.; Castellano, F. N.; Li, X.; Chen, L. X. Revealing Excited-State Trajectories on Potential Energy Surfaces with Atomic Resolution in Real Time. *Angewandte Chemie International Edition* **2023**, *62* (28), e202304615. https://doi.org/10.1002/anie.202304615.

(61) Okuniewski, A.; Rosiak, D.; Chojnacki, J.; Becker, B. Coordination Polymers and Molecular Structures among Complexes of Mercury(II) Halides with Selected 1-Benzoylthioureas. *Polyhedron* **2015**, *90*, 47–57. https://doi.org/10.1016/j.poly.2015.01.035.

(62) Swierk, J. R. The Cost of Quantum Yield. *Org. Process Res. Dev.* **2023**, *27* (7), 1411–1419. https://doi.org/10.1021/acs.oprd.3c00167.

(63) Cagan, D. A.; Bím, D.; Silva, B.; Kazmierczak, N. P.; McNicholas, B. J.; Hadt, R. G. Elucidating the Mechanism of Excited-State Bond Homolysis in Nickel–Bipyridine Photoredox Catalysts. *J. Am. Chem. Soc.* **2022**, *144* (14), 6516–6531. https://doi.org/10.1021/jacs.2c01356.

(64) Barth, A. T.; Pyrch, A. J.; McCormick, C. T.; Danilov, E. O.; Castellano, F. N. Excited State Bond Homolysis of Vanadium(V) Photocatalysts for Alkoxy Radical Generation. *J. Phys. Chem. A* **2024**, *128* (36), 7609–7619. https://doi.org/10.1021/acs.jpca.4c04250.

(65) Hwang, S. J.; Anderson, B. L.; Powers, D. C.; Maher, A. G.; Hadt, R. G.; Nocera, D. G. Halogen Photoelimination from Monomeric Nickel(III) Complexes Enabled by the Secondary Coordination Sphere. *Organometallics* **2015**, *34* (19), 4766–4774. https://doi.org/10.1021/acs.organomet.5b00568.

(66) Campbell, B. M.; Gordon, J. B.; Raguram, E. R.; Reynolds, K. G.; Sullivan, M. G.; Nocera, D. G. Ligand-to-Metal Charge Transfer of Ag(II) CF2X Carboxylates: Quantum Yield and Electrophotocatalytic Arene Fluoroalkylation Tuned by X. *Angewandte Chemie* **2025**, *137* (37), e202511642. https://doi.org/10.1002/ange.202511642.

(67) Weiss, R.; Kudisch, B. Ultrafast Nonradiative Relaxation Limits the Efficiency of Photoinduced Bond Homolysis in Molecular LMCT Photocatalysts. *J. Am. Chem. Soc.* **2025**, 147, 40264. https://pubs.acs.org/doi/10.1021/jacs.5c10766